Quantitative estimation of the impact of European teleconnections on interannual variation of East Asian winter temperature and monsoon

Young-Kwon Lim[1] and Hae-Dong Kim[2]

[1] NASA Goddard Space Flight Center, Goddard Earth Sciences Technology and Research (GESTAR), I. M. System Group, Maryland, U.S.A.

(Email: Young-Kwon.Lim@nasa.gov)

[2] College of Environment, Keimyung University, Daegu, South Korea

(Email: khd@kmu.ac.kr)

January 28, 2014

Submitted to Journal of Climate

Abstract

The impact of European teleconnections including the East Atlantic/West Russia (EA/WR), the Scandinavia (SCA), and the East Atlantic (EA) on East Asian winter temperature variability was quantified and compared with the combined effect of the Arctic Oscillation (AO), the Western Pacific (WP), and the El-Niño Southern Oscillation (ENSO), which are originated in the Northern Hemispheric high-latitudes or the Pacific. Three European teleconnections explained 22–25% of the total monthly upper-tropospheric height variance over Eurasia. Regression analysis revealed warming by EA/WR and EA and cooling by SCA over mid-latitude East Asia during their positive phase and vice versa. Temperature anomalies were largely explained by the advective temperature change process at the lower troposphere. The average spatial correlation over East Asia (90–180°E, 10–80°N) for the last 34 winters between observed and reconstructed temperature comprised of AO, WP and ENSO effect (AWE) was ~0.55, and adding the European teleconnection components (ESE) to the reconstructed temperature improved the correlation up to ~0.64. Lower level atmospheric structure demonstrated that approximately five of the last 34 winters were significantly better explained by ESE than AWE to determine East Asian seasonal winter temperatures. We also compared the impact between EA/WR and AO on the 1) East Asian winter monsoon, 2) cold surge, and 3) the Siberian high. These three were strongly coupled, and their spatial features and interannual variation were somewhat better explained by EA/WR than AO. Results suggest that the EA/WR impact must be treated more importantly than previously thought for a better understanding of East Asian winter temperature and monsoon variability.

1. Introduction

The impact of planetary-scale circulation patterns (i.e., teleconnection) on East Asian winter temperature variability have been explored in many studies primarily focusing on the Arctic Oscillation (AO) (Jeong and Ho 2005; Park et al. 2011) or El Niño Southern Oscillation (ENSO) (Chen et al. 2004). However, recent studies argue the decreasing role of ENSO (He et al. 2013) and increasing role of other large-scale patterns to influence East Asian winter temperatures. For example, Lim et al. (2012) and Liu et al. (2012) found the importance of the Arctic sea ice variation to drive an anomalously warm or cold winter over East Asian region. Another important factor that possibly affects East Asian winter temperature is the teleconnection patterns originating in the North Atlantic. Several studies have suggested the possible impact of the European teleconnections on East Asian winter climate variability (Bueh and Nakamura 2009; Wang et al. 2011). The East Atlantic/West Russia (EA/WR) (Barnston and Livezey 1987; Washington et al. 2000), Scandinavia (SCA) (Wallace and Gutzler 1981), and East Atlantic (EA) (Bojariu and Reverdin 2002) patterns are examples of European teleconnections suggesting to affect East Asian winter temperatures. However, their importance in determining East Asian winter temperatures has not attracted any significant or detailed investigations. Few studies have critically examined the responsible dynamic mechanism and assessed the significance of their impacts, compared with the relatively well-understood impacts originating from the Pacific (e.g., the Western Pacific (WP) and the ENSO) or the Northern hemispheric high-latitudes (e.g., AO).

The AO is understood to be a dominant teleconnection resolving East Asian winter monsoon (EAWM) variability (Gong et al. 2001; Li and Yang 2010). However, Wang et al.

(2011) suggested the possible role of EA/WR in modulating EAWM variability. That study found a correlated structure between meridional wind anomalies over East Asia in winter and sea surface temperatures in the preceding summer over the North Atlantic, where the study presumed was the source region for the EA/WR-like teleconnection pattern. We also suggest that the large-scale pressure anomaly in central Russia driven by the EA/WR can affect the EAWM significantly. This pressure pattern is strongly related to the Siberian high, and as commented in Wu and Wang (2002b), this Siberian high may not be necessarily dependent on the AO for influencing the EAWM. It would be worthwhile to compare the strength of the EA/WR impact with the AO impact on East Asian winter temperatures including winter monsoon.

The present study was motivated by the lack of understanding of the possible role of European teleconnections in modulating East Asian winter temperatures and monsoon variability. In this study, we intended to clarify whether the European teleconnections are one of the dominant components comprising large-scale climate variability over East Asia. Their impact was then quantitatively estimated through regression, correlation, and a temperature advective process (Linkin and Nigam 2008) to better identify their role in determining anomalous winter temperatures over East Asia. The degree of their contribution to East Asian winter temperature was also compared with the combined effects of AO, WP, and ENSO. Particularly, the impact of EA/WR and AO, respectively, on EAWM activity was compared to better identify their importance to modulate East Asian winter climate variability.

Section 2 describes the dataset and analysis method used in this study. Estimation of the impact of European teleconnections and their comparison with the impact of AO, WP

and ENSO are addressed in Section 3. Section 3 also compares the strength between the impact of EA/WR and AO on EAWM activity and the related cold surge, followed by concluding remarks and discussion in Section 4.

2. Data and methods

The primary analytical methods utilized in this study are the rotated empirical orthogonal function (REOF) technique (Richman 1986) and linear regression. The REOF was applied to upper-tropospheric monthly height archived at the Modern Era Retrospective analysis for Research and Applications (MERRA) reanalysis (Rienecker et al. 2011). The analysis time period covers the past 34 winters from December-February (DJF) 1979/80 through DJF 2012/13. Horizontal resolution of the data is 0.5° (latitude) × 0.6667° (longitude). Lower-level (850 hPa) wind and temperature data were used to investigate the thermal advective process over the East Asian domain. We also used 2 meter level MERRA temperature data to compare temperature anomalies induced by the impact of European teleconnections with the observed temperature anomalies. Several indices were used, including the East Asian winter monsoon index (EAWMI) (Jhun and Lee 2004; Li and Yang 2010), the cold surge index (CSI) (Chang et al. 2005) and the Siberian high index (SHI) (Panagiotopoulos et al. 2005) to investigate the impact of EA/WR and AO on interannual variation of EAWM and the cold surge.

3. Results

a. Impact of European teleconnections

Dominant large-scale teleconnection patterns were captured using the upper level (250 hPa) geopotential height for the domain that spans Europe and Asia. The monthly climatological cycle of the height field for DJF was removed and the REOF technique was applied to capture the leading teleconnection patterns. Three European teleconnection patterns that show height anomalies over East Asia (left panel in Fig. 1) were identified, as well as patterns originating in the Pacific or the Northern hemispheric high-latitude such as AO (right panel in Fig. 1). Anomalies are plotted on a positive phase basis in Fig. 1. The sum of their percentage variance tended to be sensitive to a slight domain change, but it varied within the range of 45–50%. We compared the principal component (PC) time series with the corresponding teleconnection time series available from the National Center for Environmental Prediction (NCEP)/Climate Prediction Center (CPC) (ftp://ftp.cpc.ncep.noaa.gov/wd52dg/data/indices/tele_index.nh) to confirm if teleconnection patterns captured here are reliable. We found that the PC and teleconnection time series are highly correlated (>0.7).

The EA/WR pattern in Figure 1a consists of two large-scale anomalies over Europe located in Western Europe and Russia north of the Caspian Sea (Barnston and Livezey 1987; Washington et al 2000; Wang et al 2011) and an anomaly over the mid-latitude Asian sector. The pattern appears to have a large-scale wave propagation structure spanning the Atlantic, Europe, western Russia, and East Asia. The positive height anomaly over East Asia north of 40°N with the negative anomaly south of it implies anticyclonic circulation with the easterly anomaly from the Pacific along 35–40°N during the positive phase, whereas the opposite is true for the negative phase.

The SCA pattern shows height anomalies of the opposite sign occurring over the Scandinavian Peninsula, and southern and eastern Europe (Fig. 1b) (Wallace and Gutzler 1981). In addition to the Scandinavian Peninsula and mid-latitude Europe (Bueh and Nakamura 2007), the anomaly values over continental Asia indicate the possible SCA impact on Asian winter climate variability.

Figure 1c shows the EA pattern characterized by strong north-south dipole anomalies over the southern part of Europe (Sáenz et al 2001; Bojariu and Reverdin 2002). A positive anomaly over the western part of continental Asia and a negative anomaly around China and Mongolia are found, though their magnitudes are smaller than those over the Atlantic. The southerly wind anomaly can be dominant along the eastern side of the negative height anomaly over China, transporting a warm air mass to the eastern China, Korea, and Japan during this positive EA phase.

Spatial distribution of the AO consists of the zonally symmetric alternating anomalies in the Arctic and the Northern Hemispheric mid-latitudes (Fig. 1d) (Thompson and Wallace 1998). It is clear that an easterly anomaly crossing the southern part of Japan and Korea is feasible during the positive phase, whereas the negative phase favors a westerly anomaly along mid-latitude East Asia (30–40°N) that could transport a continental cold air mass to this region.

Figure 1e represents the WP pattern (Wallace and Gutzler 1981; Mo and Livezey 1986; Barnston and Livezey 1987) characterized by a north-south dipole of height (or pressure) anomalies over the northwestern Pacific. East Asian winter climate can be influenced by circulation on the western side of these height anomalies. Additionally, the meridional pressure gradient during the WP event can modulate intensity of upper-level westerlies

(Linkin and Nigam 2008). The height field associated with ENSO in Fig. 1f exhibits a broad positive height anomaly distribution over the East Asian mid-latitudes (30–50°N) and negative anomaly over the southeastern China during an El Niño episode, whereas the opposite response will be true for the La Niña phase.

Actual temperature anomalies associated with each European teleconnection (EA/WR, SCA and EA) were quantitatively estimated by regressing the monthly 2 meter air temperature anomalies onto the monthly teleconnection time series. Figure 2a shows a positive temperature response to the positive EA/WR, spanning Northern China, Mongolia, Russia near Lake Baikal, Korea and Japan, whereas a cold temperature response is true for the negative EA/WR. Specifically, the impact of EA/WR tends to be strong in Russia near Lake Baikal with a temperature magnitude greater than 1K. With the magnitude smaller than 1K, the areas affected by EA/WR with a statistical significance over East Asian mid-latitudes are Korea, Japan and northern China north of 35°N.

Figure 2b clearly shows that nearly all Eurasia regions have a negative temperature anomaly during the positive SCA. The SCA impact reaches East Asia including the southeastern part of China. Negative temperature anomalies in the range of −1K–−0.5K are found over northern China, Mongolia, and northern Korea, whereas a negative temperature response smaller than that is distributed over Korea, Japan, and eastern China south of 40°N. In contrast, a weak positive temperature response < 0.5K is found over the southeastern part of China.

The temperature pattern associated with the positive EA in Fig. 2c demonstrates wide coverage of the EA impact spanning East Asia, as the influence over the Korean Peninsula was suggested in Kim et al. (2012). The sign and magnitude of the anomaly is comparable

to that of EA/WR, exhibiting a value greater (less) than 0.5K over the region north (south) of ~40°N.

The right panels in Fig. 2 represent the regressed lower-level (850 hPa) temperature advection [K day^{-1}] and circulation associated with each teleconnection. Advective temperature change is calculated by $-V_{Tel} \cdot \nabla T_{Cli}$ (Linkin and Nigam 2008). V_{Tel} represents the regressed horizontal winds related to each teleconnection, whereas T_{Cli} are the monthly climatological temperatures. The contribution of the nonlinear component, $-V_{Tel} \cdot \nabla T_{Tel}$, and the other linear component, $-V_{Cli} \cdot \nabla T_{Tel}$, was ignored because their values are an order of magnitude smaller than $-V_{Tel} \cdot \nabla T_{Cli}$. Figure 2d reveals that an anticyclonic circulation was dominant during the positive EA/WR phase over the mid-latitude East Asia and the western Pacific, where a positive height anomaly is seen in Fig. 1a. Favorable conditions for a southerly wind anomaly developed, leading to a warm advection anomaly over vast areas of East Asia covering Mongolia, China, Korea, and Japan. During the positive SCA, the atmosphere is characterized by cold advection with a relatively weak northerly wind anomaly over East Asia (Fig. 2e). In contrast, warm advection in conjunction with southwesterly anomaly is observed over the southeastern China area with statistical significance. The impact of positive EA is a warming over most of East Asian domain, similar to the impact of a positive EA/WR. Figure 2f reveals that warm advection and a southerly wind anomaly is dominant, linked to the eastern side of negative height anomaly and the western side of the positive height anomaly over East Asia found in Fig. 1c.

The magnitude of wind vectors over East Asia is generally smaller than those over the Siberian region because East Asia is situated in the far eastern side of the downstream

region of European teleconnections, where the eastward wave propagation associated with the teleconnections could likely weaken (Bueh and Nakamura 2007; Wang et al 2011; Lim and Kim 2013). However, wind anomalies appear strong enough to influence winter temperature variability over East Asia, as illustrated in Fig. 2. Note that the temperature anomaly and circulation in the event of the negative teleconnection phase can be understood in an opposite manner. The cooling effect by EA/WR and EA and the warming effect by SCA are feasible during their negative episodes.

b. Comparison of the impact of European teleconnections with AO, WP, and ENSO

Figures 1 and 2 strongly demonstrate that East Asian winter temperature variability is determined not only by the combined effect of AO, WP, and ENSO (referred to as AWE), but also by the European teleconnections (referred to as ESE). Here, we reconstructed the three sets of monthly temperature data. One set contains the impacts of both AWE and ESE, another contains the ESE effect only, and the other contains the AWE effect only. Data reconstruction was completed by linear combination of the regressed temperature anomalies and corresponding teleconnection time series. We then calculated the spatial correlation between the reconstructed temperatures and observed temperature anomalies in each year for the domain covering East Asia (90–180°E, 10–80°N). Figure 3a is a time series of the resulting spatial correlation values over all 34 winters. The red line representing the correlation of temperatures due to AWE impact with the observations reveals reasonable reproduction of the observed East Asian winter temperature variability, producing a correlation average of 0.55 over all 34 winters. The blue line representing the ESE impact has a correlation average of 0.51. More critical inspection of these time series

identified several winters such as 1982–83, 1989–90, 1996–97, 2003–04, 2004–05, 2008–09, and 2011–12 when the observed temperatures were rather poorly reproduced by the AWE impact (see the red line with correlations < ~0.4 for those seven winters). Of these seven winters, observed temperatures during five winters, except 1989–90 and 2008-09, were much better explained when both the AWE and ESE impacts were considered, as the black line reflecting the combined effect of both AWE and ESE revealed improved correlation values for those five winters. The correlation value due to the AWE impact was only 0.04 on average for those five winters and the correlation significantly increased up to 0.65 after considering both the AWE and ESE impacts. Over all 34 winters, the time series in black, representing the combined effect of AWE and ESE, improved the correlation average to 0.64 from 0.55, which is the correlation due to the AWE impact only.

Figure 3b–3g illustrate that observed temperature distributions (Figs. 3d and 3g) are remarkably better explained by considering both the AWE and ESE impacts for the selected two year cases (1996–97 and 2011–12) mentioned in the previous paragraph (Figures 3b and 3e) rather than considering the AWE impact only. Our analysis for the other winter cases of 1982–83, 2003–04, and 2004–05 support this conclusion (figure not shown). However, the remaining winters (28–29 winters) do not exhibit a significantly greater correlation when both AWE and ESE impacts are considered, compared with considering only the AWE impact, as shown in Fig. 3a (see similar correlation values denoted by black and red for many winter cases). This result indicates that although the ESE impact is important to significantly improve the correlation obtained by considering AWE impact only, that significant improvement does not occur for all years. Many winter

cases reveal that the observed temperature was reasonably reproduced by AWE impacts without a substantial addition of ESE impacts.

Atmospheric structures of lower-level temperature advection and circulation due to the ESE impact (left panel in Fig. 4) and AWE impact (right panel in Fig. 4), respectively, were compared for the three selected winters (1996–97, 2003–04 and 2011–12) to more clearly demonstrate that the ESE impact sometimes play a crucial role in reliably explaining the observed temperature distribution shown in Fig. 3. The spatial distribution of temperature advection by the ESE impact for 1996–97 (Fig. 4a) and 2011–12 (Fig. 4c) better reproduces the observed temperature distribution (Figs. 3d and 3g) than the pattern caused by the AWE impact shown in Figs. 4d and 4f. Specifically, the 2011–12 winter was severely cold (Fig. 3g) over East Asia and seemed to be a result of European teleconnections that enhanced cold advection (compare Figs. 4c and 4f). Additionally, the 2003–04 winter was recorded as an anomalously warm winter over East Asia (http://www.ncdc.noaa.gov/temp-and-precip/global-maps.php) and this observational feature was better explained by ESE impacts, as warm advection was found over continental East Asia in Fig. 4b but it was not in Fig. 4e (AWE impacts).

c. Impact of teleconnection on East Asian winter monsoon and cold surge

East Asian winter temperature is largely influenced by frequency and intensity of cold surges, which are closely linked to the EAWM. Previous studies have argued a dominant role of AO in determining the EAWM activity and cold surge (Gong et al. 2001; Park et al. 2011). Park et al. (2011) also addressed, however, that occurrence of cold surge in the form of wave train was little related to the AO phase, indicating that we still need a clarification

whether or not the AO phase is a predominant factor to determine EAWM activity and the cold surge over East Asia. In this section, we compared the impact of AO with the impact of EA/WR on 1) East Asian winter monsoon, 2) the cold surge and 3) the Siberian high to verify if the impact of AO is really the most dominant factor to determine variation in those three features. We first defined the EAWM index (EAWMI) (Fig. 5, red-solid line) following Jhun and Lee (2004) and Li and Yang (2010) based on variations in the upper-level westerly jet over East Asia. We found that those two indices were very highly correlated ($r = 0.87$). Table 1 shows temporal correlations between teleconnection indices (EA/WR and AO) and EAWMI time series. Negative correlation values indicate a strong EAWM during the negative phase of EA/WR and AO, and vice versa. It is clear that EAWMI has a stronger negative correlation with the EA/WR (−0.59) than with the AO (−0.24). Stronger negative correlations with the EA/WR are also found for the cold surge index (CSI) (Fig. 5, red-dashed line) and the Siberian high index (SHI) (Fig. 5, red-dotted line), which will be discussed in more detail later. Figure 5 shows that all indices (EAWMI, CSI, SHI, –EA/WR and –AO) exhibit upward trends for the periods ~1988/89–2012/13 winter. Calculating the correlation after removing this linear upward trend over the ~25 winters once again produced a stronger negative correlation with the EA/WR (~−0.35) than with the AO (~-−0.10), which is no longer significant. This low correlation with the AO is consistent with Jhun and Lee (2004) and Wu et al. (2006) who suggested little correlation between AO and EAWM on an interannual time scale.

Atmospheric spatial patterns regressed onto the EAWMI were calculated and then compared with those regressed onto the negative phase of EA/WR and AO, respectively. Figure 6 clearly shows that strong EAWM over East Asia is characterized by below

average temperature (Fig. 6a), northerly flow coming from Siberia and the northwestern Pacific (Fig. 6b), enhanced upper-level westerly in mid-latitudes (~20°–40°N) (Fig. 6c) and upper-level continental convergence and oceanic divergence (Fig. 6d). The spatial distributions of these patterns are quite close to the regressed patterns associated with the negative EA/WR shown in Figs. 7a–c. The temperature distribution in Fig. 6a also significantly resembles the pattern in Fig. 2a multiplied by −1, indicating a strong EAWM during the negative EA/WR and vice versa. Figures 7d–f represents the negative AO impact and exhibit similar spatial distributions to those associated with EAWMI (Fig. 6), but the similarity between them is relatively weaker than that between the negative EA/WR (Figs. 7a–c) and EAWMI (Fig. 6). For example, the magnitude of upper level westerly anomalies and their locations shown in Fig. 6c are better explained by Fig. 7b than by Fig. 7e. The pressure distribution with the sea-land contrast and large-scale anomaly centered over Siberia seen in Fig. 6b is better reproduced by Fig. 7a than by Fig. 7d. Upper-level divergent/convergent flow between the Asian continent and the northwestern Pacific, which is a typical characteristic of large-scale monsoon circulation, is also better structured in Fig. 7c than in Fig. 7f. These characteristic differences imply a connection between EAWM and EA/WR comparable to or closer than a connection between EAWM and AO. Spatial correlations (90°–150°E and 20°–60°N) in Table 2 clarifies that EAWM activity has closer connection with the phase of EA/WR than with the AO. These results are somewhat different from several studies that argued the most dominant role for AO in determining the EAWM intensity (e.g., Gong et al. 2001; Wu and Wang 2002a). However, Gong et al. (2001) also suggested a significant contribution of the Eurasian teleconnection pattern (e.g., EA/WR) to better explain the interannual variation of EAWM and the Siberian high.

EAWM activity is also understood to be an indicator of cold surge activity (Jhun and Lee 2004; Li and Yang 2010). Chang et al. (2005) defined CSI for the South China Sea and southeastern Asia using the meridional wind component. We applied that definition to the mid-latitudes for the domain of 90°–130°E and 40°–60°N, which covers northeastern Asia and the eastern side of Siberian high. The CSI was defined as the area-averaged meridional wind over this spatial domain (Fig. 5, red-dashed line). This region was selected because it is a good pathway for the meridional wind coming from the Northern high-latitudes toward mid-latitude East Asia. Note that merigional wind components were multiplied by −1 so that the CSI value is positive during the cold surge year and vice versa. Regressed patterns associated with the CSI were found to resemble Fig. 6, demonstrating that the EAWM is an indicator of cold surge activity over East Asia (Fig. 8). The temporal correlation between CSI and EAWMI is 0.77. Table 3 clearly demonstrates a stronger relationship between the cold surge and negative EA/WR than with the negative AO, which is a good agreement with the conclusion in Table 2.

The reason for the higher correlation between the EAWMI and CSI with the EA/WR than with the AO seems to be associated with a better representation of the Siberian high pressure variation due to the impact of EA/WR than AO. This, in turn, indicates that the Siberian high may not be closely linked to the AO (Wu and Wang 2002b). For confirmation, we calculated the Siberian high index (SHI) following Panagiotopoulos et al. (2005) and Hasanean et al. (2013) and then examined its correlation with the EA/WR and AO, respectively.

The temporal correlation between SHI vs. CSI and SHI vs. EAWMI is 0.81 and 0.69, respectively, over the last 34 winters, indicating that the Siberian high is strongly coupled

with the winter monsoon and cold winters over East Asia (Gong and Ho 2002). The spatial distributions regressed onto SHI shown in Fig. 9 are nearly consistent with the patterns regressed onto EAWMI (Fig. 6). Spatial correlations (90°–150°E and 20°–60°N) between SHI and two teleconnections (EA/WR and AO) shown in Table 4 demonstrate that EA/WR better represents the variation in the Siberian high than that of AO. Cheung et al. (2012) described the dominant role of Ural-Siberian blocking for influencing the EAWM. The pressure pattern associated with the blocking (Fig. 3a in Cheung et al. (2012)) resembled the typical pattern of EA/WR over Russia. Our results support the arguments by several studies that the impact of AO alone does not faithfully explain the variation of Siberian high (Wu and Wang 2002b) and the EAWM activity on an interannual time scale (Jhun and Lee 2004).

4. Conclusion and discussion

We investigated the impacts of European teleconnections (ESE: EA/WR, SCA, and EA) on East Asian winter temperature variability focusing on quantifying their impacts and comparing with the impact of AWE (AO, WP and ENSO). The sum of ESE and AWE explained 45–50% of the total monthly upper-troposphere height variance over Eurasia with 22–25% each. Statistically significant temperature anomalies, which are associated with one standard deviation in each teleconnection time series based on linear regression, were found with a 0.5–1K amplitude over mid-latitude East Asia. We found that these temperature anomalies were largely explained by the advective temperature change process at the lower atmospheric level. Of the last 34 winters, five (1982–83, 1996–97, 2003–04,

2004–05, and 2011–12) exhibited significantly better reproduction of the observed seasonal temperature anomalies due to the impact of ESE than that by AWE.

It appears that ESE's overwhelming impact was often found when the strength of the AO impact was weaker than average. The average amplitude of the AO indices obtained from the NCEP/CPC for those five winters was 0.40 with a maximum of 0.98 (2003–04 winter), whereas the average over all 34 winters was 0.90.

We also determined that the conventional understanding that AO is the most dominant teleconnection to affect the EAWM may need to be re-evaluated. The comparison between the impact of EA/WR and AO on the EAWM activity, the cold surge and the Siberian high provided consistent results that the EA/WR tends to better represent their interannual variation. The EA/WR modulates the variation in the Siberian high more effectively than that of the AO. As evidenced by correlations and regressed patterns in this study, variations in the Siberian high and corresponding monsoon circulation, which leads to a warmer/colder winter over East Asia, was more accurately reproduced by the EA/WR impact, though the AO impact also explained them reasonably.

In this study, the North Atlantic Oscillation (NAO) was also captured as one of the dominant REOF modes over the Eurasian domain. However, we did not consider the NAO because of the very small magnitude of the regressed temperature anomalies over mid-latitude East Asia. This is in agreement with Wang et al. (2005) who addressed regionality of the NAO impact. As a result, no significant temperature anomalies were produced over East Asia. Thus, the NAO contributed little to the interannual temperature variability and spatial correlation discussed in Figure 3. Additionally, the calculated spatial correlations with the EAWMI, CSI and SHI-associated patterns (Table 1 through 4) produced lower

correlation coefficients with the NAO (correlations not shown) than with any other teleconnection. Jhun and Lee (2004) and Hong et al. (2008) suggested that the impact of NAO is more related to the decadal-scale East Asian cold extreme variability or EAWM rather than to interannual time-scale variability. Decadal-scale variation was not fully examined in this study due to the limited analysis period. Nonetheless, the evidence presented here indicated that the ESE impact, particularly the EA/WR, needs to be treated more importantly than previously thought for a better understanding of the interannual variations in East Asian winter temperature and monsoon.

Acknowledgement

This research was supported by the Scholar Research Grant of Keimyung University in 2013.

References

Barnston, A. G., and R. E. Livezey, 1987: Classification, seasonality and persistence of low-frequency atmospheric circulation patterns. *Mon. Wea. Rev.,* **115,** 1083-1126.

Bojariu, R., and G. Reverdin, 2002: Large-scale variability modes of freshwater flux and precipitation over the Atlantic. *Clim. Dyn*., **18,** 369-381.

Bueh, C., and H. Nakamura, 2007: Scandinavian pattern and its climate impact. *Quart. J. Royal. Meteor. Sci.,* **133,** 2117-2131.

Chen, T.-C., W.-R. Huang, and J.-H. Yoon, 2004: Interannual variation of the East Asian cold surge activity. *J. Climate*, **17,** 401-413.

Gong, D.-Y., S.-W. Wang, and J.-H. Zhu, 2001: East Asian winter monsoon and Arctic Oscillation. *Geophys. Res. Lett*., **28**, 2073-2076.

Gong, D.-Y., and C.-H. Ho, 2002: Siberian high and climate change over middle to high latitude Asia. *Theor. App. Climatol*., **72**, 1-9.

Hasanean, H. M., M. Almazroui, P. D. Jones, and A. A. Alamoudi, 2013: Siberian high variability and its teleconnectios with tropical circulations and surface air temperature over Saudi Arabia. *Clim. Dyn*., **41**, 2003-2018, doi:10.1007/s00382-012-1657-9.

He, S., H. Wang, and J. Liu, 2013: Changes in the relationship between ENSO and Asia-Pacific midlatitude winter atmospheric circulation. *J. Climate*, **26,** 3377-3393.

Hong, C.-C., H.-H. Hsu, H.-H. Chia, and C.-Y. Wu, 2008: Decadal relationship between the North Atlantic Oscillation and cold surge frequency in Taiwan. *Geophys. Res. Lett*., **35,** L24707, doi:10.1029/2008GL034766.

Jeong, J.-H., and C.-H. Ho, 2005: Changes in occurrence of cold surges over East Asia in association with Arctic Oscillation. *Geophys. Res. Lett*., **32,** L14704, doi:10.1029/2005GL023024.

Jhun, J.-G., and E.-J. Lee, 2004: A new East Asian winter monsoon index and associated characteristics of the winter monsoon. *J. Climate*, **17**, 711-726.

Kim, J.-S., S. Jain, and Y.-I. Moon, 2012: Atmospheric teleconnection-based conditional streamflow distributions for the Han River and its sub-watersheds in Korea. *Int. J. Climatol.,* **32,** 1466-1474.

Li, Y., and S. Yang, 2010: A dynamical index for the East Asian winter monsoon. *J. Climate*, **23**, 4255-4262.

Lim, Y.-K., Y.-G. Ham, J.-H. Jeong, and J.-S. Kug, 2012: Improvement in simulation of Eurasian winter climate variability with realistic Arctic sea ice condition in an atmospheric GCM. *Env. Res. Lett*., **7,** 044041(6pp) doi:10.1088/1748-9326/7/4/044041.

Lim, Y.-K., and H.-D. Kim, 2013: Impact of the dominant large-scale teleconnections on winter temperaturevariability over East Asia. *J. Geophys. Res. Atmos*., **118,** 7835–7848, doi:10.1002/jgrd.50462.

Linkin, M. E., and S. Nigam, 2008: The North Pacific Oscillation – West Pacific teleconnection pattern: mature-phase structure and winter impacts. *J. Climate,* **21,** 1979-1997.

Liu, J., J. A. Curry, H. Wang, M. Song, and R. M. Horton, 2012: Impact of declining Arctic sea ice on winter snowfall. *PNAS,* **109,** 4074-4079.

Mo, K. C., and R. E. Livezey, 1986: Tropical-extratropical geopotential height teleconnections during the northern hemisphere winter. *Mon. Wea. Rev.*, **114,** 2488-2515.

Panagiotopoulos, F., M. Shahgedanova, A. Hannachi, and D. Stephenson, 2005: Observed trends and teleconnections of the Siberian High. *J. Climate*, **18**, 1411-1422.

Park, T.-W., C.-H. Ho, and S. Yang, 2011: Relationship between the Arctic Oscillation and cold surges over East Asia. *J. Climate,* **24**, 688-83.

Richman, M. B., 1986: Rotation of principal components. *J. Climatol*., **6**, 293–335.

Rienecker, M. M., and Coauthors, 2011: MERRA – NASA's Modern-Era Retrospective Analysis for Research Applications. *J. Climate,* **24**, 3624-3648.

Sáenz, J., C. Rodríguez-Puebla, J. Fernández, and J. Zubillaga, 2001: Interpretation of interannual winter temperature variations over southwestern Europe. *J. Geophys. Res*., **106**, D18, 20641-20651.

Thompson, D. W. J., and J. M. Wallace, 1998: The Arctic oscillation signature in the wintertime geopotential height and temperature fields. *Geophys. Res. Lett., **25***(**9)**, 1297–1300, doi:10.1029/98GL00950.

Wang, D., C. Wang, X. Yang, and J. Lu, 2005: Winter Northern Hemisphere surface air temperature variability associated with the Arctic Oscillation and North Atlantic Oscillation. *Geophys. Res. Lett.*, **32**, L16706, doi:10.1029/2005GL022952.

Wang, X., C. Wang, W. Zhou, D. Wang, and J. Song, 2011: Teleconnected influence of North Atlantic sea surface temperature on the El Niño onset. *Clim. Dyn*., **37**, 663-676, DOI:10.1007/s00382-010-0833-z.

Wallace, J. M., and D. S. Gutzler, 1981: Teleconnections in the geopotential height field during the Northern Hemisphere winter. *Mon. Wea. Rev.,* **109**, 784–812.

Washington, R., A. Hodson, E. Isaksson, and O. Macdonald, 2000: Northern hemisphere teleconnection indices and the mass balance of Svalbard glaciers. *Int. J. Climatol*., **20**, 473-487.

Wu, B., and J. Wang, 2002a: Possible impacts of winter Arctic Oscillation on Siberian high, the East Asian winter monsoon and sea-ice extent. *Advan. Atmos. Sci*., **19**, 297-320.

Wu, B., and J. Wang, 2002b: Winter Arctic Oscillation, Siberian high and East Asian winter monsoon. *Geophys. Res. Lett*., **29**, 1897, doi:10.1029/2002GL015373

Wu, B., R. Zhang, and R. D'Arrigo, 2006: Distinct modes of the East Asian winter monsoon. *Mon. Wea. Rev*., **134**, 2165-2179.

Table 1 Temporal correlation between the East Asian winter monsoon index (EAWMI), cold surge index (CSI), Siberian high index (SHI), respectively, with teleconnection indices (EA/WR and AO)

	EA/WR	AO
EAWMI	-0.59	-0.24
CSI	-0.54	-0.27
SHI	-0.57	-0.21

Table 2 Spatial correlation between the pattern associated with the East Asian winter monsoon index and teleconnection (EA/WR and AO)

	T2m	UV850	SLP	U300	Velp
EAWMI .vs. EA/WR	-0.87	-0.86	-0.97	-0.92	-0.86
EAWMI .vs. AO	-0.66	-0.62	-0.56	-0.59	-0.72

Table 3 Spatial correlation between the pattern associated with the cold surge index and the teleconnection (EA/WR and AO)

	T2m	UV850	SLP	U300	Velp
CSI .vs. EA/WR	-0.85	-0.84	-0.95	-0.92	-0.91
CSI .vs. AO	-0.60	-0.57	-0.54	-0.60	-0.68

Table 4 Spatial correlation between the pattern associated with the Siberian high index and the teleconnection (EA/WR and AO)

	T2m	UV850	SLP	U300	Velp
SHI .vs. EA/WR	-0.92	-0.69	-0.97	-0.95	-0.71
SHI .vs. AO	-0.74	-0.62	-0.53	-0.65	-0.65

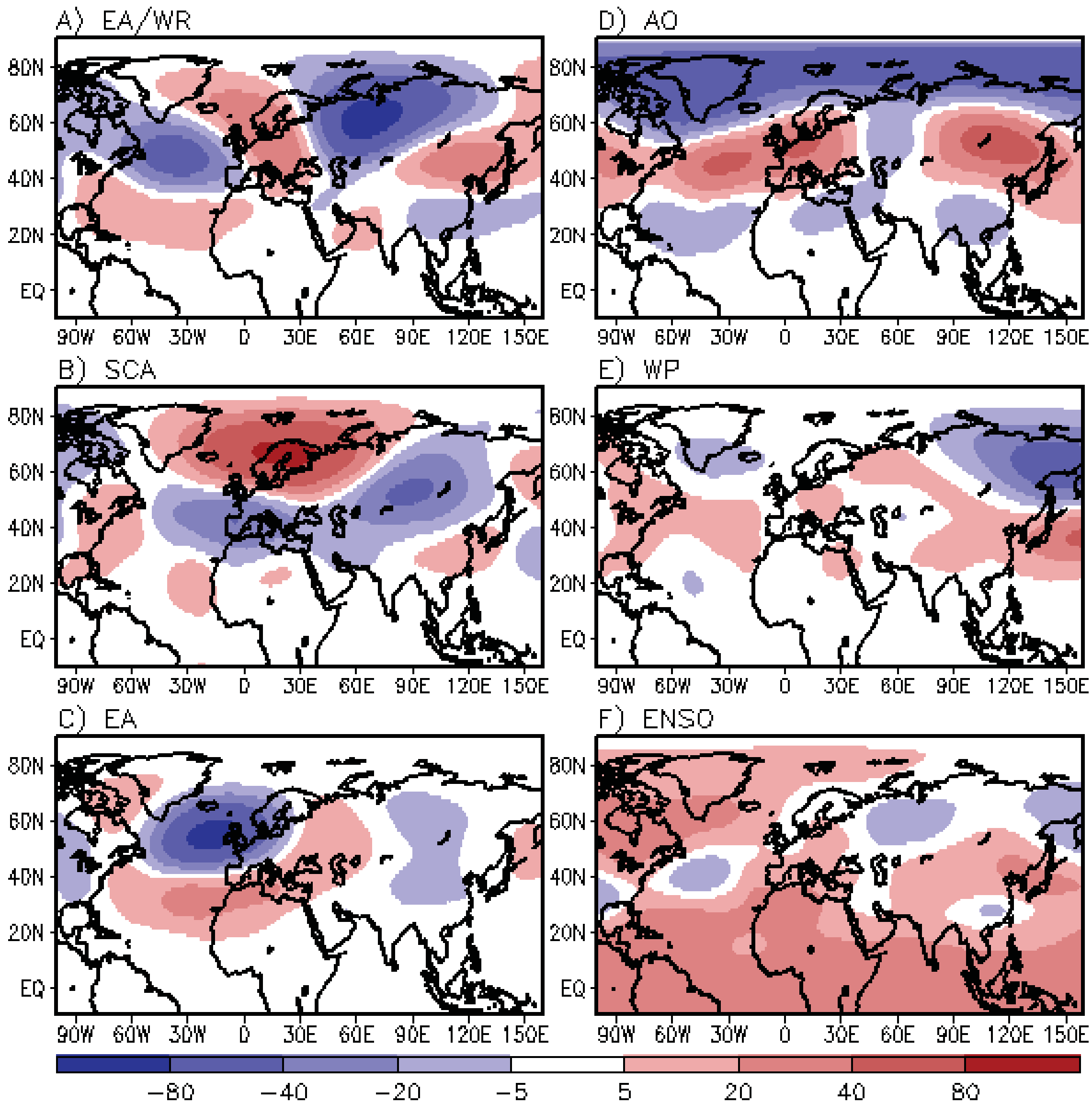

Figure 1. The non-normalized rotated empirical orthogonal functions (REOFs) of the monthly 250 hPa height [m] archived from a MERRA reanalysis. The analysis period included the last 34 winters from December–February (DJF) 1979/80 through DJF 2012/13. The left panel represents the distribution of European teleconnections (East Atlantic/West Russia, Scandinavia, and East Atlantic) whereas the right panel represents the Arctic Oscillation, the Western Pacific, and the El-Niño Southern Oscillation.

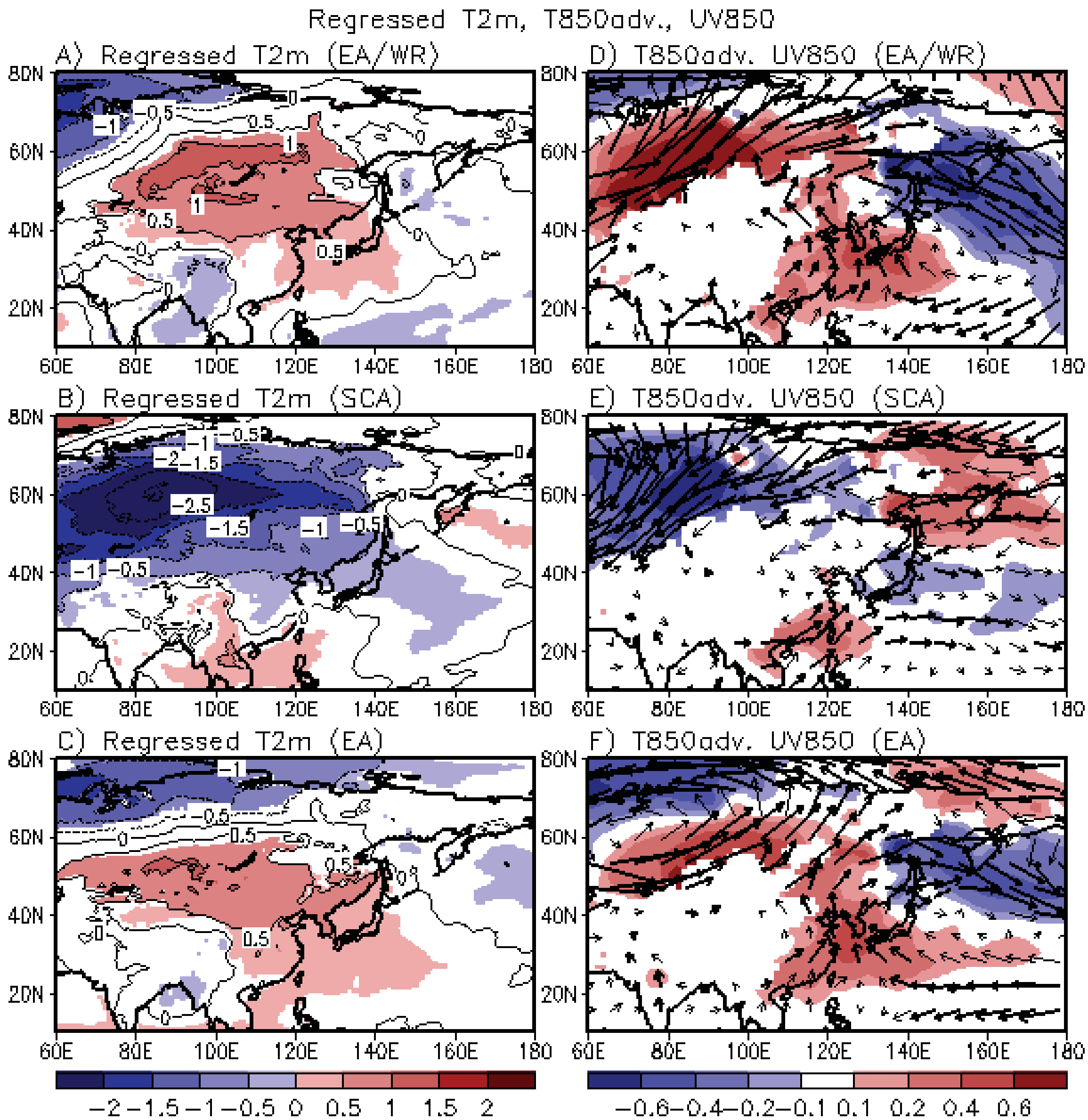

Figure 2. Distribution of the 2 meter air temperature anomalies (left panel) [K] and the atmospheric circulation and advective temperature change ($-V_{Tel} \cdot \nabla T_{Cli}$) [K day^{-1}] at 850 hPa (right panel) associated with one standard deviation in each European teleconnection time series based on linear regression. Shaded regions are where the anomaly values are statistically significant at 10%. Wind vectors statistically significant at 10% level are plotted as thick lines. V_{Tel} denotes the regressed horizontal winds, and T_{Cli} represents the climatological monthly temperatures. Note that the high-elevation region in continental Asia such as western China and the Tibetan area is treated as missing in the right panel.

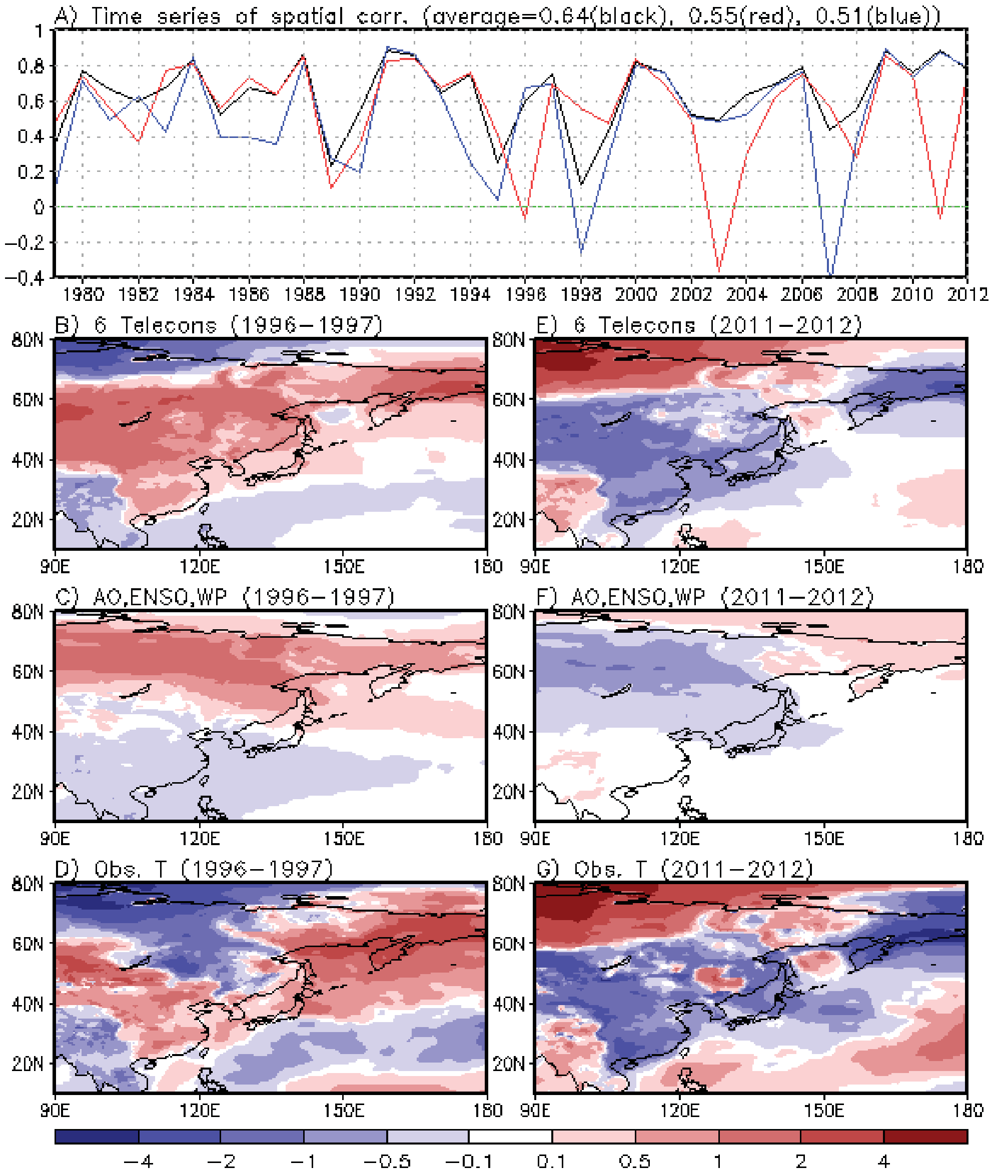

Figure 3. Upper: Time series of the spatial correlation coefficients between observed temperature anomalies (temporal anomalies) and the reconstructed temperatures comprised of both AWE and ESE impacts (black), ESE impact (blue), and AWE impact (red), respectively, for the geographic domain shown in the lower panels. B) and E) represent the winter temperature anomalies by the combined effect of AWE and ESE for 1996–97 (B) and 2011–12 (E), respectively. C) and F) are the same as B) and E) but for the anomalies caused by the impact of AWE. Observed temperature anomaly distributions for those years are shown in D) and G) for comparison.

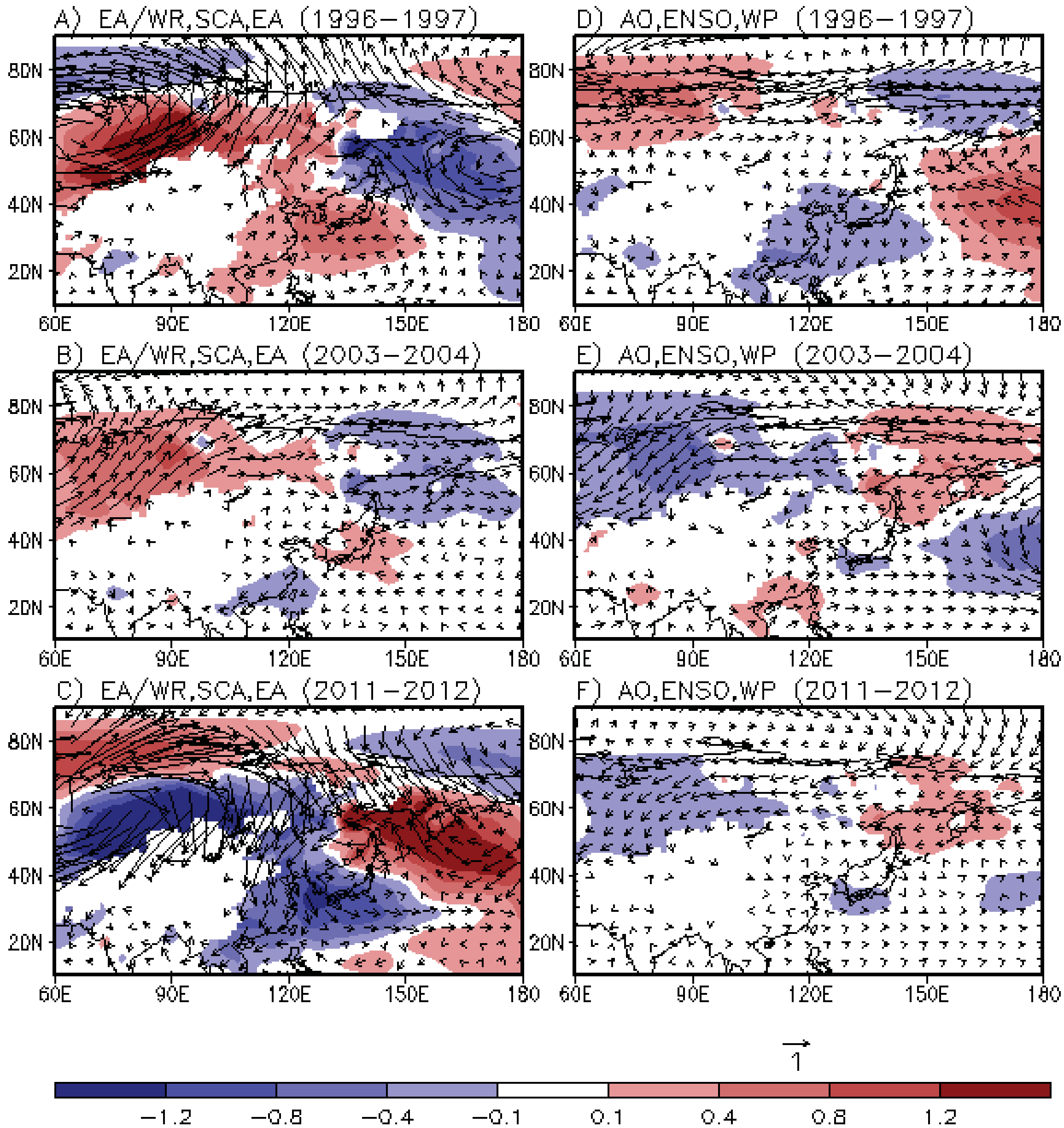

Figure 4. Distribution of the atmospheric circulation and advective temperature change ($-V_{Tel} \cdot \nabla T_{Cli}$) [K day^{-1}] at 850 hPa caused by the impact of ESE (left panel) and AWE (right panel) for the three selected winter cases (1996–97, 2003–04, and 2011–12). Note that the high-elevation region in continental Asia such as western China and the Tibetan area is treated as missing.

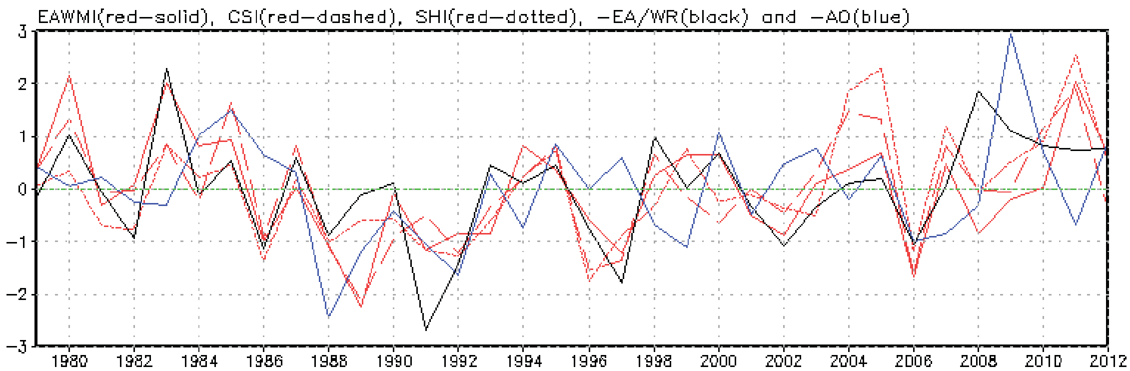

Figure 5. Interannual variation in normalized EAWMI, CSI, SHI, –EA/WR, and –AO. They are denoted by red-solid, red-dashed, red-dotted, black solid, and blue solid line, respectively.

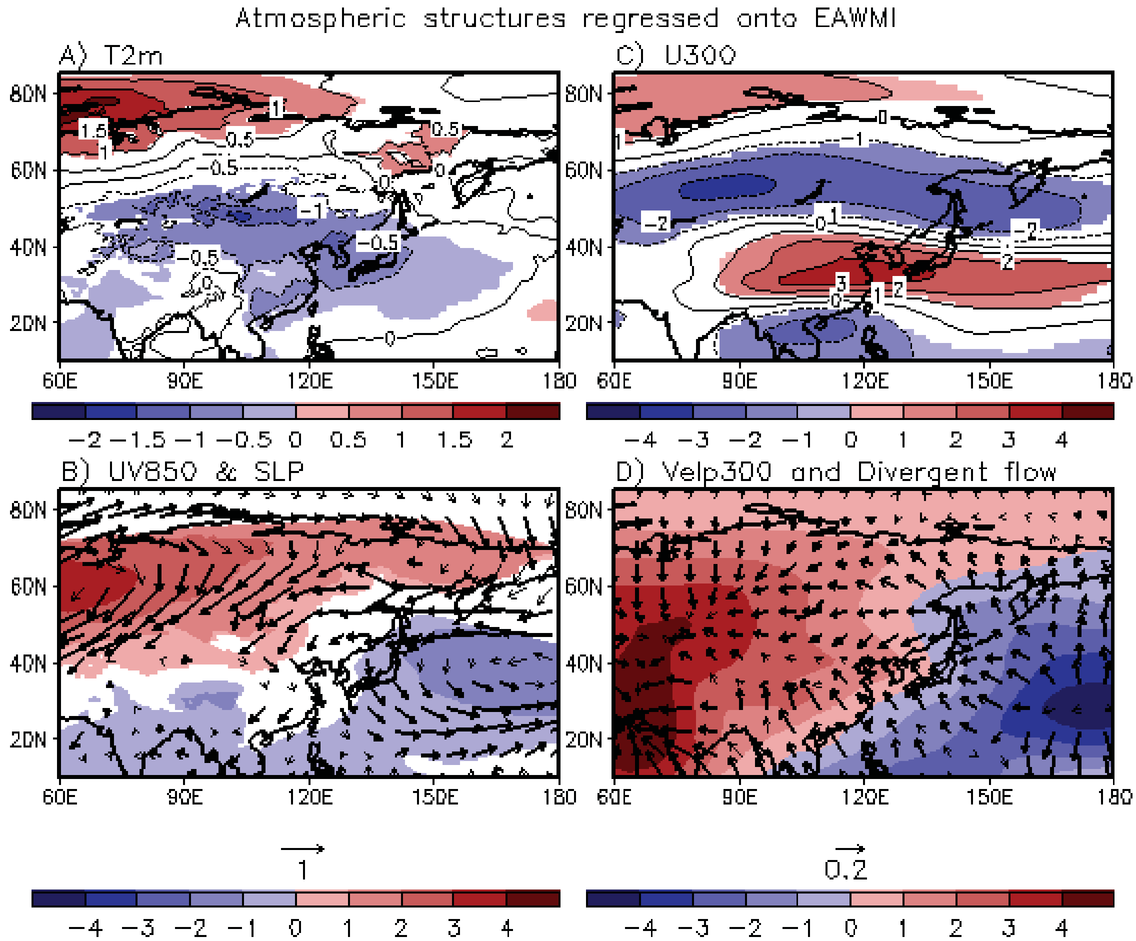

Figure 6. Horizontal distributions of atmospheric variables regressed onto EAWMI. Except velocity potential [1.0e+5 m^2s^{-1}] on the lower-right panel, the shaded area indicates where the values are significant at the 10% level. Thick arrows on the bottom panel (B and D) indicate vectors significant at the10% level.

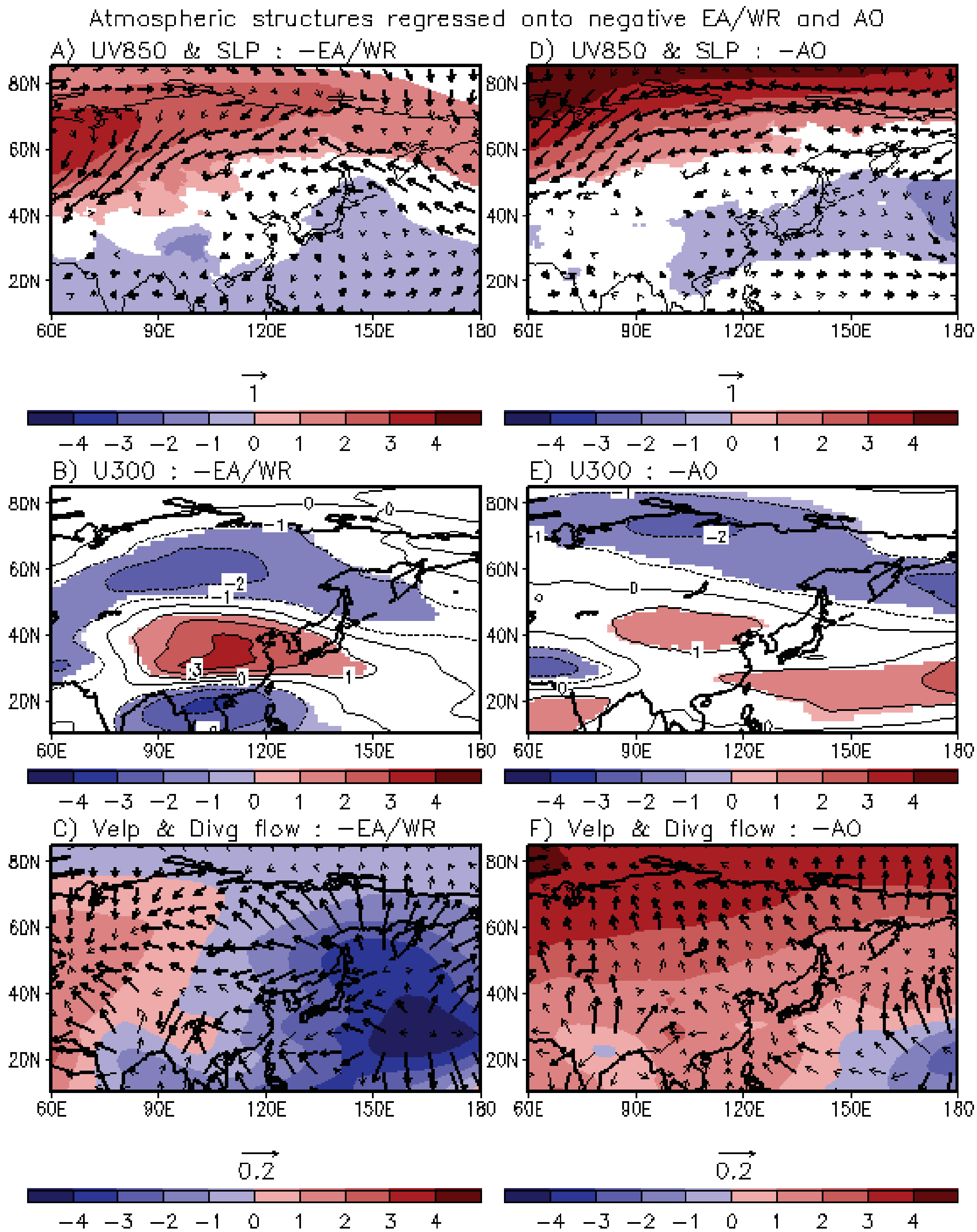

Figure 7. Horizontal distributions of atmospheric variables regressed onto –EA/WR (left) and –AO (right). Except velocity potential [$1.0e+5\ m^2s^{-1}$] on the bottom panel (C and F), shaded area indicates where values are significant at the 10% level. Thick arrows on the top (A and D) and bottom panel (C and F) indicate vectors significant at the 10% level.

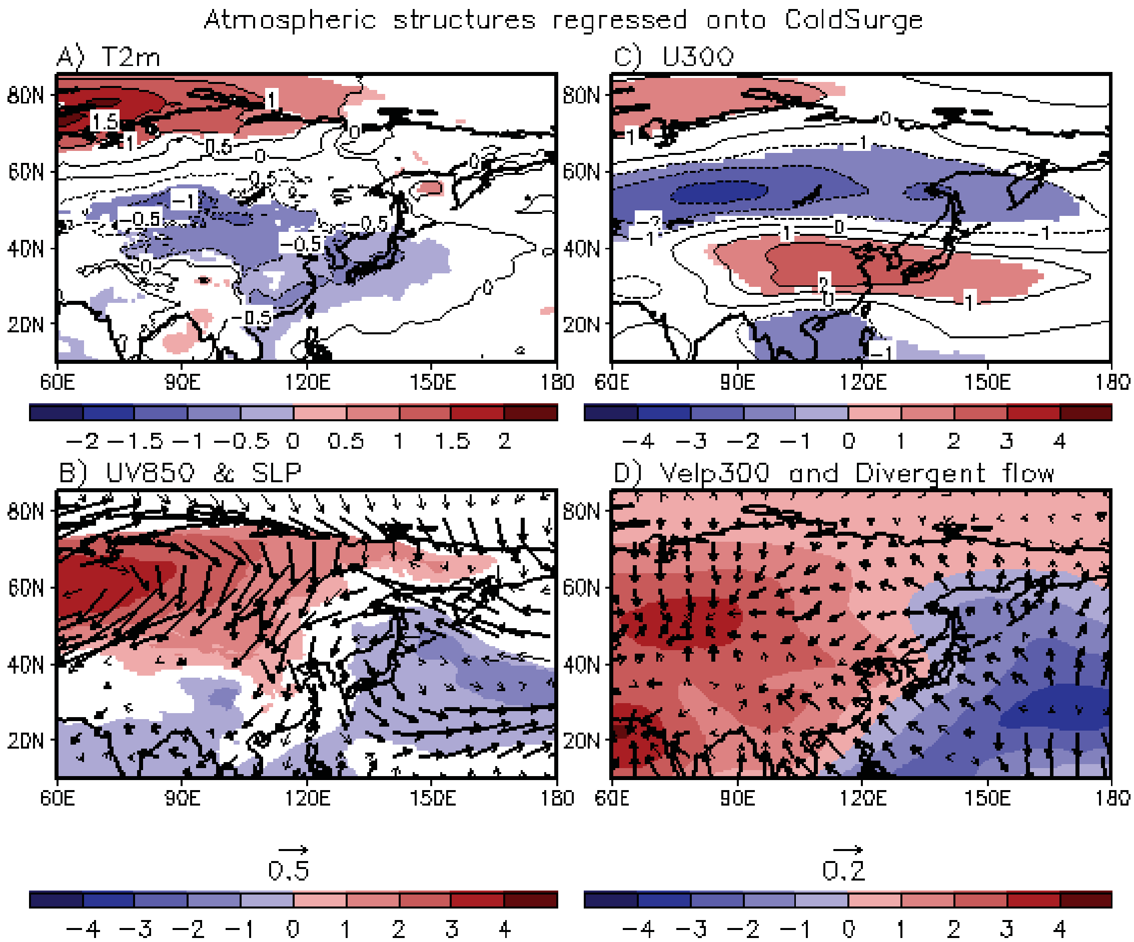

Figure 8. Same as Figure 6 but for regression onto CSI.

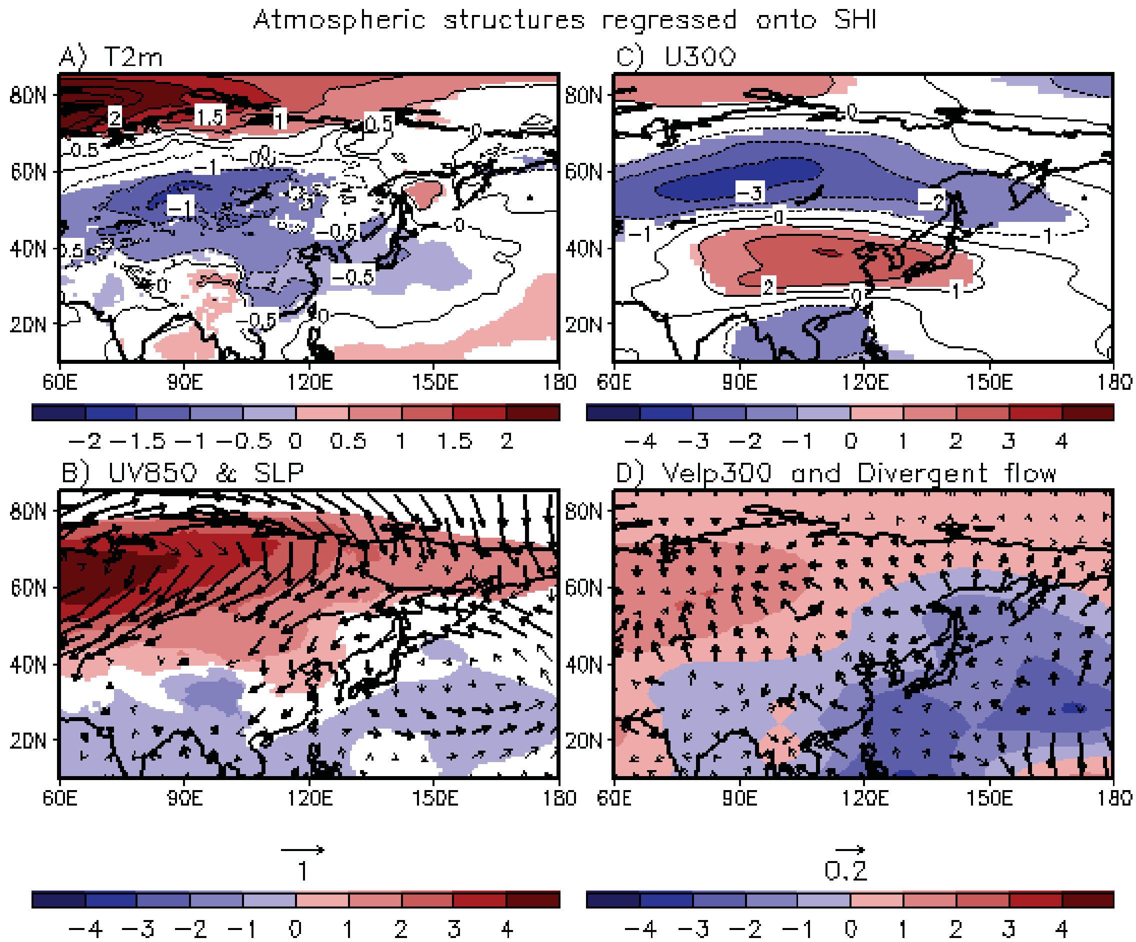

Figure 9. Same as Figure 6 but for regression onto SHI.